Zweitveröffentlichung/
Secondary Publication

Staats- und
Universitätsbibliothek
Bremen

https://media.suub.uni-bremen.de

Almeida, Renato S.M. ; Farhandi, Hedieh ; Tushtev, Kamen ; Rezwan, Kurosch

Enhancing thermal stability of oxide ceramic matrix composites via matrix doping

Journal Article as: peer-reviewed accepted version (Postprint)

DOI of this document*(secondary publication): https://doi.org/10.26092/elib/3260

Publication date of this document: 06/09/2024

* for better findability or for reliable citation

Recommended Citation (primary publication/Version of Record) incl. DOI:

Renato S.M. Almeida, Hedieh Farhandi, Kamen Tushtev, Kurosch Rezwan,
Enhancing thermal stability of oxide ceramic matrix composites via matrix doping,
Journal of the European Ceramic Society, Volume 42, Issue 7, 2022, Pages 3282-3289,
ISSN 0955-2219, https://doi.org/10.1016/j.jeurceramsoc.2022.02.040.

Please note that the version of this document may differ from the final published version (Version of Record/primary publication) in terms of copy-editing, pagination, publication date and DOI. Please cite the version that you actually used. Before citing, you are also advised to check the publisher's website for any subsequent corrections or retractions (see also https://retractionwatch.com/).

This document is made available under a Creative Commons licence.

The license information is available online: https://creativecommons.org/licenses/by-nc-nd/4.0/

Take down policy

If you believe that this document or any material on this site infringes copyright, please contact publizieren@suub.uni-bremen.de with full details and we will remove access to the material.

Enhancing thermal stability of oxide ceramic matrix composites via matrix doping

Renato S.M. Almeida [a], Hedieh Farhandi [a], Kamen Tushtev [a,*], Kurosch Rezwan [a,b]

[a] *Advanced Ceramics, Universität Bremen, Bremen 28359, Germany*
[b] *MAPEX - Center for Materials and Processes, Universität Bremen, Bremen 28359, Germany*

ARTICLE INFO

Keywords:
Ceramic matrix composites
Nextel 610
Alumina
Magnesia
Grain growth

ABSTRACT

To overcome the main limitation of oxide ceramic matrix composites (Ox-CMCs) regarding thermal degradation, the use of matrix doping is analyzed. Minicomposites containing Nextel 610 fibers and alumina matrices with and without MgO doping were produced. The thermal stability of the minicomposites was evaluated considering their microstructure and mechanical behavior before and after thermal exposures to 1300 °C and 1400 °C for 2 h. Before heat treatment, both composite types showed very similar microstructure and tensile strength. After heat treatment, densification, grain growth and strength loss are observed. Furthermore, the MgO dopant from the matrix diffuses into the fibers. As a result, abnormal fiber grain growth is partially suppressed and MgO-doped composites show smaller fiber grains than non-doped composites. This more refined microstructure leads to higher strength retention after the heat treatments. In summary, doping the matrix can increase the overall thermal stability without impairing the room-temperature properties of Ox-CMCs.

1. Introduction

All-oxide ceramic matrix composites (Ox-CMCs) show an interesting combination of high strength, chemical and thermal resistance, as well as high fracture toughness. Therefore, these materials are promising alternatives for high-temperature applications in oxidizing environments such as gas turbine engines, thermal protection system and hot-gas filters [1]. Ox-CMCs typically consist of alumina-based porous matrix reinforced with high-strength oxide fibers. The idea behind the use of a porous matrix is to allow for crack deflection mechanisms when the composite is mechanically loaded. In other words, possible cracks can be deflected through the matrix porosity or at fiber-matrix interface while the fibers can sustain the load [2]. Therefore, the strength of these composites is normally related to the strength of the reinforcing fibers when they are loaded on-axis. Current Ox-CMCs use mostly the alumina fiber Nextel 610 or the mullite-alumina fiber Nextel 720 as their reinforcement [1]. The high strength of these polycrystalline oxide fibers is a reflection of their refined microstructure containing nano-sized grains. To achieve that, Nextel 610 fibers have approximately 0.7 wt% of Fe_2O_3 and 0.3 wt% of SiO_2 in their chemical composition to induce the nucleation of alumina grains and to reduce grain growth during processing, respectively [3].

The main limitation of Ox-CMCs is related to their thermal stability. In general, strength reduction and embrittlement are observed when these composites are exposed to temperatures above 1000 °C [4–6]. These changes are normally associated with the further densification of the matrix and, most importantly, to the thermal degradation of the reinforcing fibers [1]. The thermal stability of oxide fibers has been extensively studied in the literature [7–11]. In the case of Nextel 610, strength reduction can be observed starting at 900 °C [10]. It is commonly accepted that fiber degradation is caused by grain growth and micro grooving [7,9,11]. Nevertheless, the extent of fiber degradation can vary when the fibers are embedded in the composites. For instance, Schmücker and Mechnich observed a more pronounced grain coarsening in the peripheral zone of Nextel 610 fibers embedded in a highly-pure alumina matrix after exposure to 1400 °C for 2 h [12]. At high temperatures, elemental diffusion and interactions between fiber and matrix can take place besides grain growth. In the aforementioned case, it was suggested that the SiO_2 dopant of the fibers diffused into the matrix. Therefore, the absence of SiO_2, which is an alumina grain growth inhibitor, resulted in higher grain growth in the fiber rim [12]. In a subsequent study, it was shown that this outward SiO_2 diffusion can be hindered if the matrix has similar chemical composition, diminishing the chemical gradient between fibers and matrix [13]. Furthermore, an

* Corresponding author.
E-mail address: tushtev@uni-bremen.de (K. Tushtev).

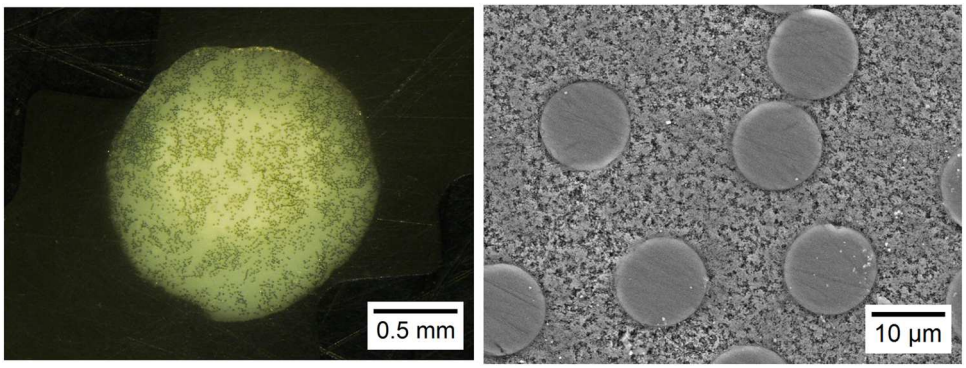

Fig. 1. Example cross-section of manufactured minicomposite sintered at 1200 °C for 2 h showing even fiber distribution.

opposite effect can also be observed if the matrix is rich in SiO_2. A study by Volkmann et al. suggests that inward SiO_2 diffusion takes place when Nextel 610 fibers are embedded in a mullite-SiOC matrix, leading to smaller grains in the fiber rim [14].

Considering that the chemical composition of the matrix can influence fiber degradation at high temperatures, the objective of this work is to investigate the applicability of matrix doping for the production of Ox-CMCs with higher thermal stability. The doping of monolithic alumina has been investigated for many years. Several doping elements are known in the literature, such as SiO_2, MgO, CaO, ZrO_2 and rare earths [15]. Although SiO_2 is commonly used for the doping of oxide fibers like Nextel 610, this dopant has a few drawbacks. For instance, SiO_2 can lead to abnormal grain growth and the formation of SiO_2 glass phase [16,17], which can impair the material`s thermal stability. Among the possible doping elements, MgO is considered one of the most effective grain growth inhibitors for alumina [18]. When used in correct amounts, MgO doping segregates at the grain boundaries of alumina and reduce the grain boundary mobility [16,18,19]. Therefore, the applicability of MgO dopant in the production of Ox-CMCs is evaluated in this study. For this purpose, Ox-CMC minicomposites were manufactured by reinforcing non-doped and MgO-doped alumina matrices with Nextel 610 fibers. The fabricated minicomposites were sintered at 1200 °C for 2 h. To evaluate the thermal stability, minicomposites were tested before and after additional heat treatments at 1300 °C and 1400 °C for 2 h. Microstructural analyses and uniaxial tensile tests were performed to investigate the influence of the dopant on the fiber degradation and on the mechanical performance of the minicomposites. Furthermore, possible fiber-matrix interactions were evaluated by wavelength-dispersive X-ray spectroscopy (WDX) analysis of selected samples.

2. Materials and methods

2.1. Specimen preparation

Minicomposites, which are unidirectional composites reinforced by fiber bundles, were fabricated and analyzed for this study. All produced minicomposites contained 3000 den Nextel 610 fiber bundles (3 M, MN, USA) as their reinforcement. The production was done using the ionotropic gelation technique [20]. For that, water-based ceramic suspensions containing a solid content of 50 vol% were prepared. For the doped minicomposites, MgO-doped alumina powder (480 ppm MgO, d_{50} = 120 nm, Baikowski, Poisy, France) was used. For comparison, another set of minicomposites was prepared using highly pure alumina powder (d_{50} = 120 nm, Baikowski, Poisy, France), i.e., non-doped minicomposites. In both cases, two alginates in the same proportion were used as the binder: Protanal LFR5/60 (FMC Corporation, Philadelphia, PA, USA) and Alginic acid sodium salt from brown algae with medium viscosity (Sigma-Aldrich Chemie GmbH, Steinheim, Germany). Detailed information about the ionotropic gelation technique for the production of Ox-CMCs can be seen in our previous publication [20]. Before the slurry infiltration, the fiber bundles were thermally desized at 700 °C for 2 h in a LHT 04/17 chamber furnace (Nabertherm GmbH, Lilienthal, Germany). Six fiber bundles were infiltrated and passed through tube-shaped paper molds to obtain minicomposites with a cylindrical shape. After drying for at least 3 days at room temperature, the paper molds were removed and the minicomposites were sintered at 1200 °C for 2 h (heating rate = 4 K/min, cooling rate = 9 K/min) in the same furnace used for fiber desizing. Fig. 1 shows an example cross section of a produced minicomposite. The minicomposites have a diameter of 1.80 ± 0.02 mm and fiber content of 19 ± 1 vol%. The samples were evaluated before (as-produced) and after heat treatments at 1300 °C and 1400 °C for 2 h. The parameters for the heat treatments were selected to represent possible applications at critical temperatures for a short time. The heat treatments were performed using the same furnace, heating and cooling rates as the ones used for sintering.

2.2. Characterization methods

The minicomposites were evaluated and compared based on their microstructure and mechanical properties. The open porosity of the minicomposites was measured by a mercury porosimeter Pascal 440 (Porotec GmbH, Hofheim am Taunus, Germany). Fiber and matrix grain sizes were measured using scanning electron microscopy (SEM) images. For that, the minicomposites were embedded in epoxy resin for grinding and polishing. Afterwards, the embedding resin was thermally extracted and the polished surfaces were thermal etched between 1100 °C and 1300 °C for 30 min. Pictures of the microstructure were taken using a ZEISS Supra 40 SEM (ZEISS, Oberkochen, Germany) with an acceleration voltage of 1 kV. Grain size measurements were performed with the software ImageJ. The ferret diameter was selected to represent the length of the grains, especially considering the abnormal grains after heat treatment. The grain size measurements were performed in the fiber center, fiber rim (at the fiber-matrix interface), as well as in the matrix region near to the fibers.

Furthermore, elemental analyses were performed using a JEOL JXA-8200 electron probe micro analyzer (JEOL Ltd., Tokyo, Japan) equipped with 5 WDX spectrometers. Sample preparation was similar to the one for the SEM images, but without performing the thermal etching. Due to the very small amount of the elements to be analyzed, e.g., 480 ppm of MgO, not all samples were tested. The measurement was focused on the sample that was expected to show the highest amount of fiber-matrix elemental diffusion: MgO-doped minicomposites after heat treatment at 1400 °C for 2 h. For comparison, an as-produced MgO-doped minicomposite was also analyzed. Pictures and element profiles were taken with an acceleration voltage of 15 kV.

The mechanical performance of the minicomposites was evaluated with uniaxial tensile tests. The tests were performed using a Kappa 050 DS universal testing machine (Zwick Roell, Ulm, Germany) equipped with a PS-E50 laser extensometer (Fiedler Optoelektrik GmbH, Lützen,

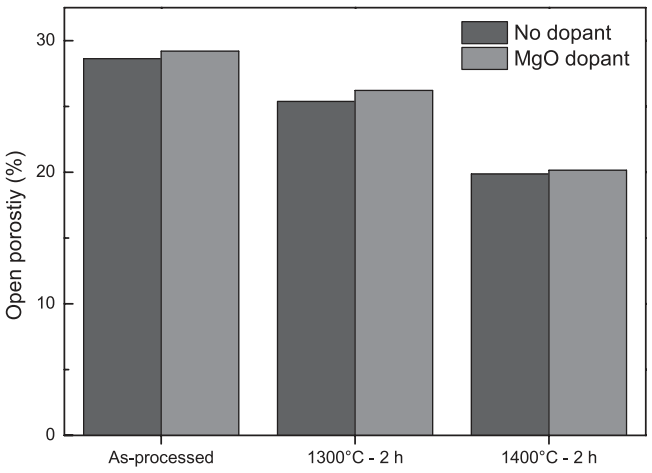

Fig. 2. Open porosity of minicomposites with and without MgO doping, before (as-processed) and after heat treatments at 1300 °C and 1400 °C for 2 h.

Germany). Five specimens per condition were tested at a constant loading rate of 0.5 mm/min. The mini-composites were clamped to the machine using conical holders. A more detailed description of the testing set-up is given in our previous publication [21]. To record the sample elongation via laser extensometer, the gauge length of 75 mm was marked in two points at a distance of 35 mm.

3. Results

3.1. Microstructural analysis

The produced minicomposites were investigated first regarding their microstructure in terms of porosity and grain size. Fig. 2 shows the measured open porosity for the minicomposites before and after the heat treatments. Considering that the fibers are highly dense, the measured open porosity is mainly related to the porosity of the matrix. Both types of minicomposite showed very similar open porosity in the as-processed state: 29.2% for MgO-doped and 28.6% for non-doped. The heat treatments have a clear influence on the porosity of the minicomposites. For instance, MgO-doped samples showed a relative porosity reduction of 10% and 31% after the 2 h heat treatment at 1300 °C and 1400 °C, respectively. A very similar trend was observed for the minicomposites without dopant. Hence, the presence of the MgO-doping does not seem to influence the further densification of the matrix at high temperatures.

Example SEM micrographs depicting the grains of fiber and matrix of non-doped and MgO-doped minicomposites are shown in Figs. 3 and 4, respectively. The micrographs were focused on the center and rim of the fibers, as well as on the matrix region close to the fiber-matrix interface. The contrast of the images was adjusted for a better visualization of the

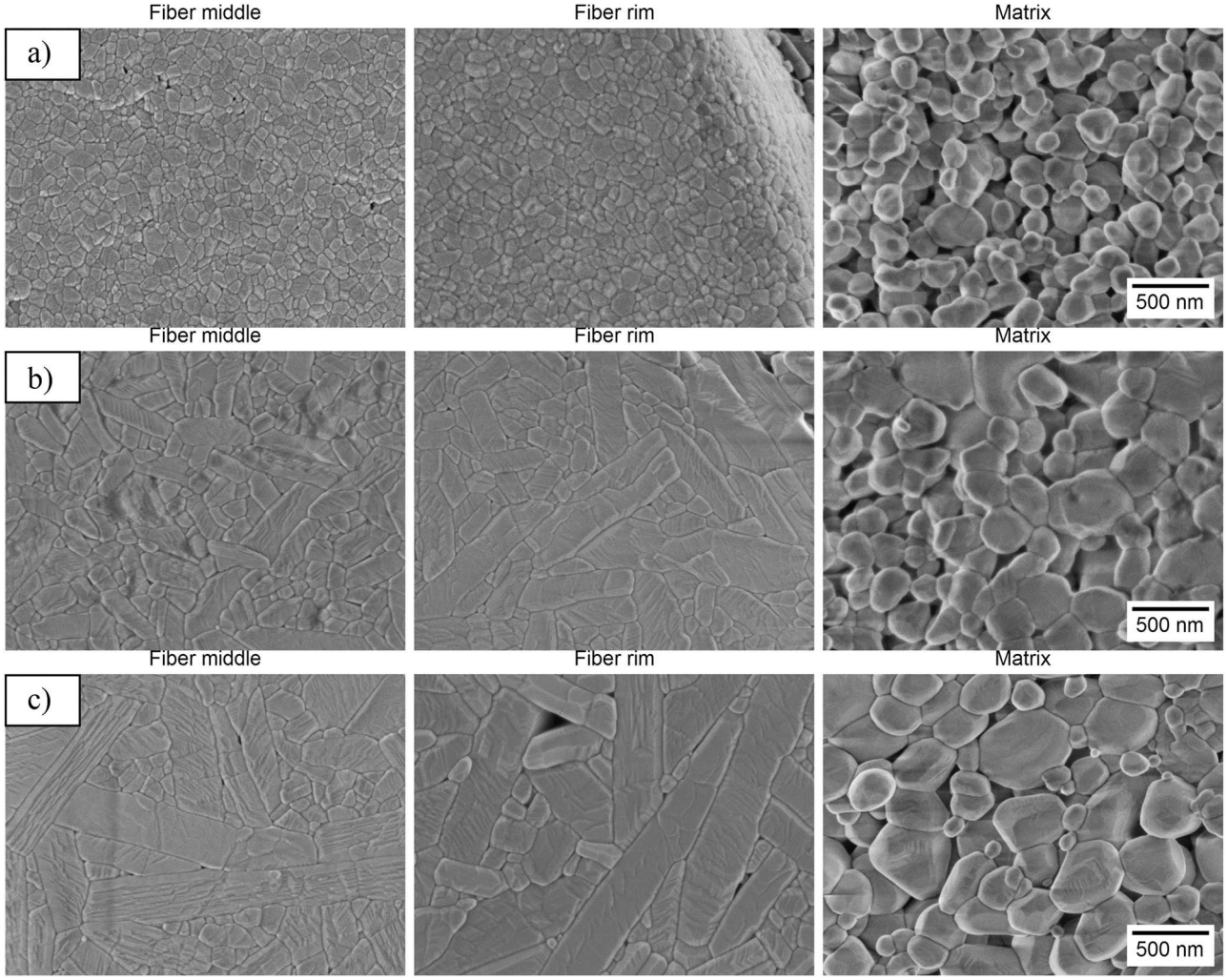

Fig. 3. SEM micrographs of non-doped minicomposites: as-processed (a) and after 2 h exposure to 1300 °C (b) and 1400 °C (c). The micrographs were taken from the fiber center, fiber rim and matrix close to the fiber-matrix interface. All micrographs have the same scale.

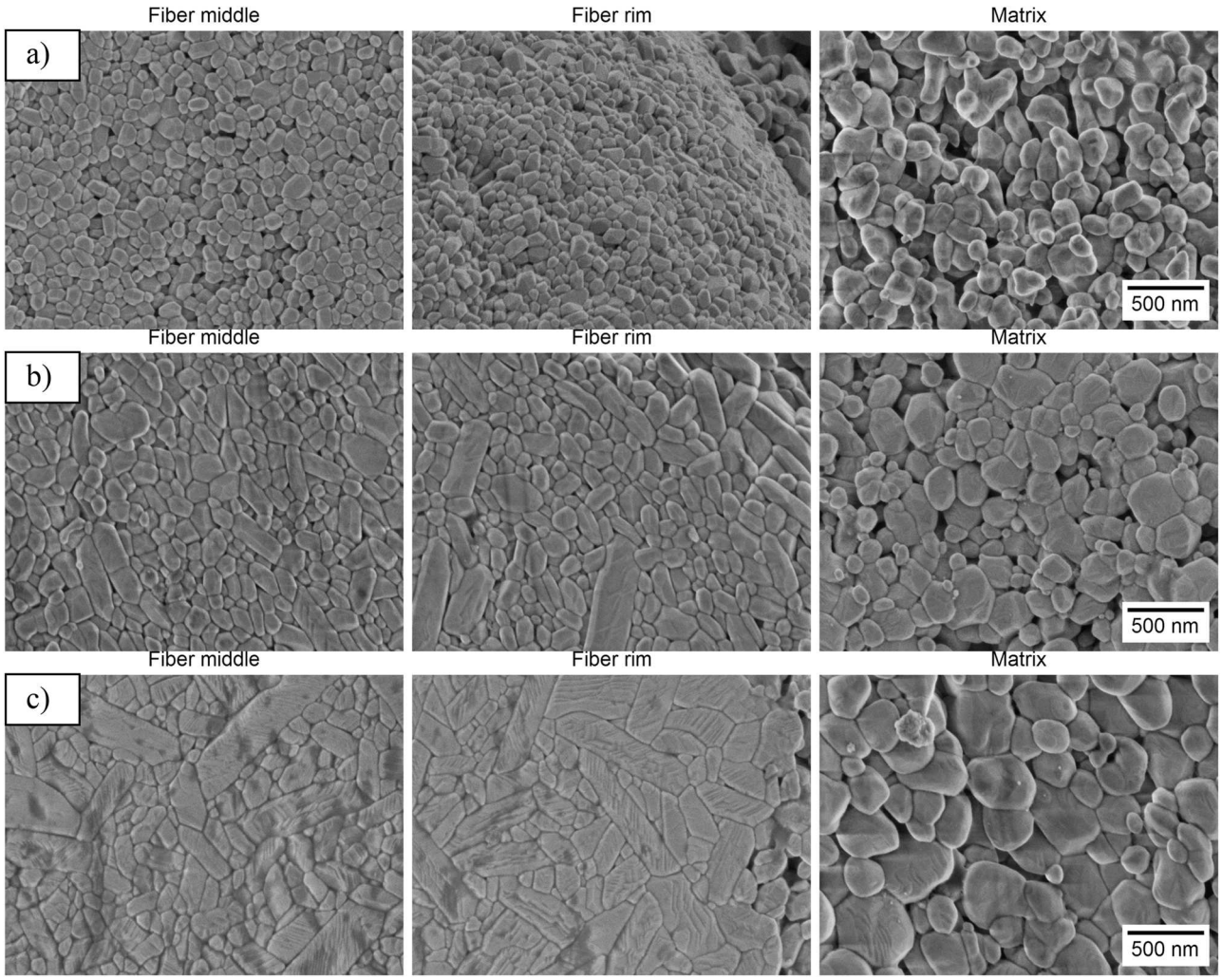

Fig. 4. SEM micrographs of MgO-doped minicomposites: as-processed (a) and after 2 h exposure to 1300 °C (b) and 1400 °C (c). The micrographs were taken from the fiber center, fiber rim and matrix close to the fiber-matrix interface. All micrographs have the same scale.

grain boundaries. In the micrograph of the fiber center in as-processed MgO-doped minicomposite (Fig. 4a), it can be seen that a few grains seem to be in a different depth. This is an indication that the sample was unfortunately not well polished, since it is relatively difficult to obtain completely flat surface during grinding and polishing considering that fiber and matrix have much different hardness due to the matrix porosity. Apart from that, both types of composites showed very similar microstructure after sintering (Figs. 3a and 4a). The grains of the fibers in both cases are mostly equiaxial and there is no apparent differences between the grains in the center and in the rim of the fibers. The same can be said for the matrix grains, although they are bigger than the fiber grains. Nevertheless, differences on fiber grains are observed after the heat treatments. Abnormal grain growth takes already after the 2 h exposure at 1300 °C as seen in Figs. 3b and 4b. In general, a higher amount of abnormal grains are observed in the fiber rim in comparison to the fiber center. This is more expressive after the heat treatment at 1400 °C (Figs. 3c and 4c), after which the elongated fiber grains are much bigger. However, smaller grains of about 100–300 nm are still observed around the abnormal grains. When comparing the minicomposite types, it is evident that the amount and size of the abnormal fiber grains are much smaller for MgO-doped samples. In contrast, the matrix grains evolution is very similar for both MgO-doped and non-doped samples. In general, the matrix grains grow, but remain relatively equiaxial.

The ferret diameter was measured to quantify the observed grain sizes. Fig. 5 shows the box plot diagrams used to graphically depict the measured grain size distributions. For each box, the lower box line denotes the first quartile, the middle line denotes the median and the upper line denotes the third quartile of the grain size distribution. The size of the box represents the distribution of the grain size data, while the filled square is the average grain size. Furthermore, the whiskers represent the maximum and minimum measured grain sizes. Here it should be noted that the maxima and minima also depend on the observation window. Additionally, scale breaks are used for better visualization of the maxima due to the abnormal grains observed after the heat treatments. As previously mentioned, the microstructures of the as-processed composites are very similar. For both cases, most of the fiber grains are within the range of 75–150 nm, while the matrix grains are around 150–250 nm. Furthermore, there are no statistical differences between the grain size distributions measured on the center and rim of the fibers.

After the heat treatments, grain growth is observed. Due to the presence of abnormal fiber grains, the grain size distributions become much wider after the heat treatments. In general, two populations of fiber grains are observed: smaller and equiaxial grains, as well as bigger elongated grains. The grain sizes distributions, measured in the fiber rim, are overall broader and have higher average in comparison to the grain size distributions of the fiber centers. When comparing the different composite types, the main observed differences are on the bigger elongated grains. For instance, after the heat treatment at 1400 °C, non-doped minicomposites showed smaller grains in the range

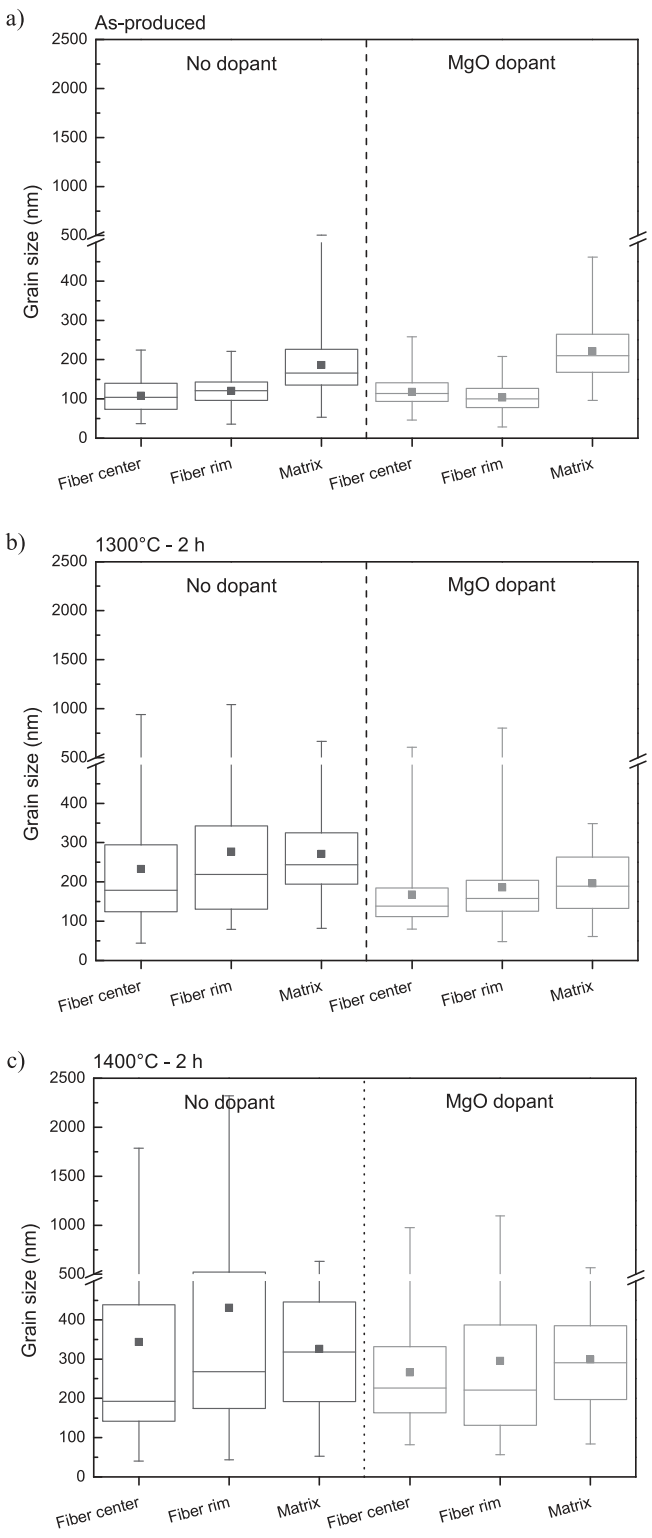

Fig. 5. Grain size distributions of non-doped and MgO-doped minicomposites: as-produced (a) and after 2 h exposures to 1300 °C (b) and 1400 °C (c). The boxes represent the first, second and third quartiles, the filled squares represent the averages and the whiskers represent the maxima and minima of the distributions.

of 125–300 nm and elongated grains ranging from 450 to 1800 nm in the fiber center. For comparison, MgO-doped minicomposites showed smaller grains in the range of 100–300 nm and elongated grains in the range of 400–1000 nm under the same conditions. In general, MgO-doped samples showed fewer elongated grains, which are also smaller in comparison to non-doped samples. As a result, fiber grain size distributions are narrower and the average grain size is smaller for MgO-doped minicomposites after the heat treatments. Two-tailed t-tests with a significance level of 0.05 were performed to assess whether the fiber grain size distributions are statistically different with and without the dopant after the thermal treatments. For all cases, the p-values were below the 0.05, indicating a significant difference between the fiber grain size distribution of doped and non-doped mini-composites after thermal treatments. On the other hand, differences are significantly smaller when comparing the matrix of doped and un-doped mini-composites under the same conditions.

3.2. *WDX elemental mapping*

Possible fiber-matrix interactions were evaluated by WDX analyses. Fig. 6 depicts the elemental distributions of Fe, Si and Mg for MgO-doped minicomposites as-processed and after the thermal exposure to 1400 °C for 2 h. In the grayscale images, the brighter regions denote higher concentration of the analyzed elements. In addition, element concentration profiles were measured between the horizontal lines in the micrographs of Fig. 6. Since Nextel 610 fibers have approximately 0.7 wt% of Fe_2O_3 and 0.3 wt% of SiO_2 in their composition [3], Fe and Si can be observed in the fiber region. However, relative differences can be seen in the concentration profiles of these elements. The concentration of Si is constant in the middle of the fiber, slowly decreasing near the fiber-matrix interface, as opposed to the abrupt drop of the concentration seen in the Fe distribution. Furthermore, the micrographs showing the Fe distribution have a well-defined perimeter of the fiber, while the perimeter is somewhat blurred for the Si distribution. This is more evident for the sample after the heat treatment at 1400 °C (Fig. 6b); indicating a possible outward diffusion of Si from the fiber to the matrix. On the other hand, Mg is barely detected in the as-processed sample. This is somewhat expected since Nextel 610 does not have Mg in its composition, and only 480 ppm of MgO were added to the matrix. However, it is interesting to see that after the heat treatment, the concentration of Mg seems to be slightly higher in the fiber than in the matrix; indicating a possible inward diffusion of Mg from the matrix to the fiber.

3.3. *Uniaxial tensile test*

The mechanical performance of the minicomposites was studied with uniaxial tensile tests. Examples of stress-strain curves for non-doped and MgO-doped minicomposites before and after the heat treatments can be seen in Fig. 7a and b, respectively. Both types of composite show similar stress-strain response having mostly linear-elastic deformation with small non-linearity before failure. Although damage can take place at relatively low stresses, no obvious elastic limit can be identified. The average tensile strength of the minicomposites before and after the heat treatments is shown in Fig. 7c. Similarly to the microstructural observations, as-processed minicomposites with and without the MgO dopant showed comparable tensile strength: 137 ± 6 MPa for non-doped and 133 ± 9 MPa for MgO-doped specimens. However, the tensile strength of the composites decrease with different intensities after the heat treatments. Non-doped specimens showed relative tensile strength reductions of 27% and 62% after exposures to 1300 °C and 1400 °C, respectively. In comparison, MgO-doped minicomposites exhibited tensile strength reductions of 8% and 41% after exposure to 1300 °C and 1400 °C, respectively.

4. Discussion

The thermal stability of Ox-CMCs depends on the microstructural changes that can happen at high temperatures. In general, oxide fibers and composites are processed at relatively low temperatures when

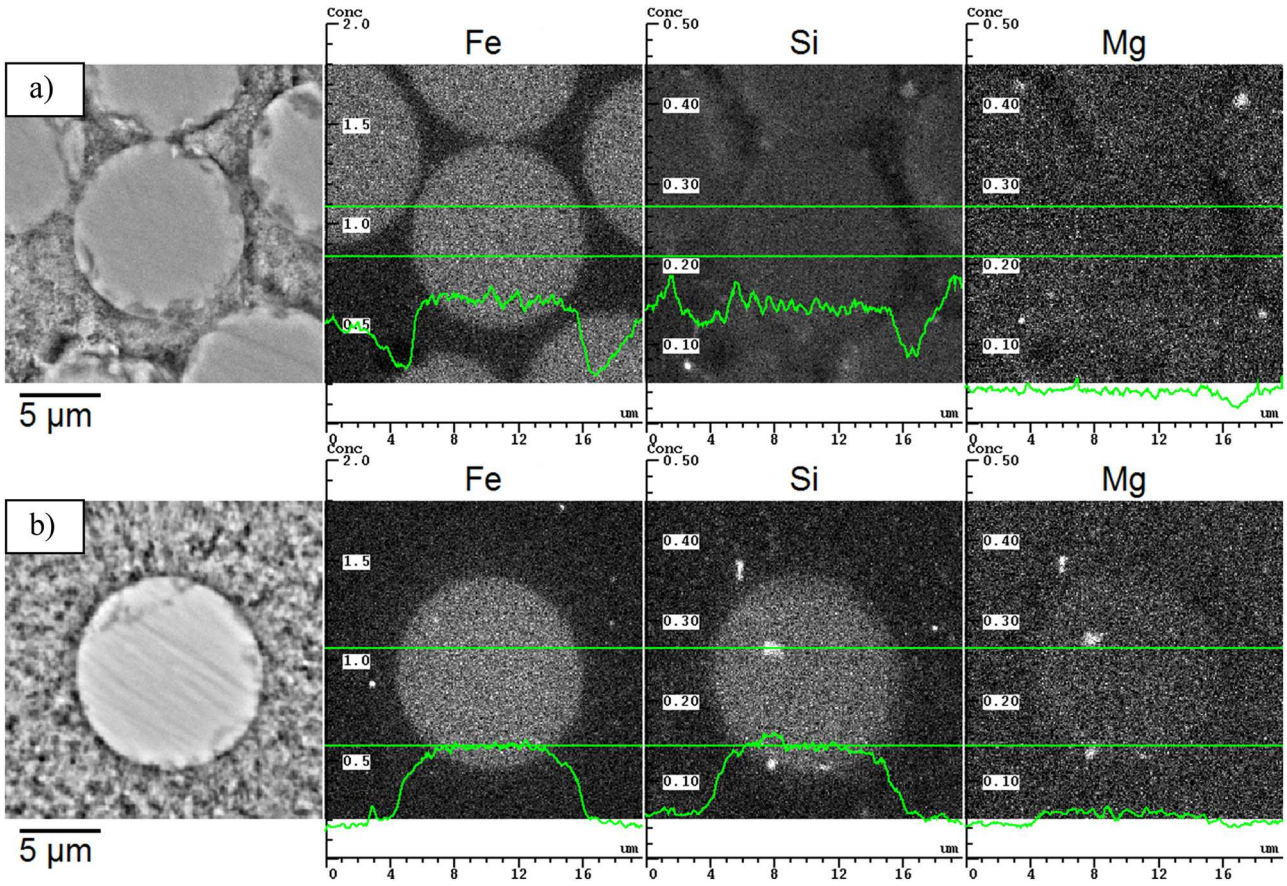

Fig. 6. WDX elemental mapping of MgO-doped minicomposites: as-processed (a) and after 2 h exposures to 1400 °C (b). Element profiles show the element concentration between the two horizontal lines.

compared to the sintering of high-density monolithic alumina. In this study for example, the sintering took place at 1200 °C for 2 h to avoid extensive fiber grain growth and achieve an open porous structure to allow for crack deflection. Hence, the used sintering parameters may be one of the reasons why minicomposites with and without doping showed very similar microstructure in the as-processed state. However, their microstructures are not completely stable when subjected to temperatures similar or above the processing conditions. Throughout the experiments, three main microstructural changes were observed after the heat treatments. Further densification of the matrix open pore structure (Fig. 2) occurs in order to reduce the surface energy. In a similar matter, grain growth is observed on both fibers and matrix (Fig. 5) due to the reduction of the grain-boundary energy. Lastly, elemental diffusion (as seen in Fig. 6) is caused by the chemical gradient between fibers and matrix. Although these phenomena have distinct driving forces, and possibly different activation energies, they all occur at the heat treatment temperatures through diffusion. In other words, they are caused by atomic movement that leads to a more stable microstructure.

The degree of these microstructural changes will depend on the diffusion rate of the atoms and species related to these mechanisms. Nevertheless, it should be highlighted that since these mechanisms might interfere with each other, their diffusion rates may also change as the microstructure develops. While densification and grain growth depend on the diffusion of Al_2O_3, albeit through different paths, elemental diffusion depends on the diffusion rate of Mg, Si and Fe species through the alumina structure. For the diffusion in alumina, metallic cations with lower valence are normally faster diffusers, while metals with higher valence show diffusion coefficients similar to the lattice elements Al and O [22]. In our previous work, it was estimated that the diffusion coefficient of Mg (valency of 2) is 6–7 times higher than of Si (valency of 4) in alumina fibers [23]. Therefore, it is safe to assume that Mg diffusion happens faster than Si diffusion, grain growth and densification (alumina diffusion). In fact, our previous investigation on phase-field modeling of Nextel 610 fibers under the same condition has shown that Mg can diffuse all the way until the center of the fiber after the 2 h exposure to 1400 °C [23]. Although the Mg concentration is very small, a similar trend can be seen in the WDX element mapping (Fig. 6b). It is also interesting that the Mg concentration seems to be slightly higher in the fiber than in the matrix after the heat treatment, even though the doping was initially in the matrix. MgO tends to segregate preferentially at grain boundaries [16,24]. Since the fibers have smaller grains and, therefore, much more grain boundaries in the as-processed state (see Figs. 4a and 5a), it is hypothesized that MgO migrates to the fibers at earlier stages. Hence, this could lead to the slightly higher Mg concentration measured after the heat treatment at 1400 °C. In contrast, Si seems to have only partially diffused from the fiber to the matrix even after the exposure to 1400 °C due to its much slower diffusion rate. As a result, Si shows higher concentration in the fiber center, which decreases at the fiber-matrix interface. Regarding the Fe_2O_3 doping of the fibers, Fe diffusion was not observed even though there is a clear Fe chemical gradient between fiber and matrix (Fig. 6). This is an indication that Fe_2O_3 is somewhat stable in the fibers, possibly forming a solid solution with Al_2O_3 [12].

As previously mentioned, the diffusion of the aforementioned elements can influence the other observed microstructural changes. SiO_2 and MgO tend to segregate at grain boundaries, limiting the atomic mobility in these regions [16]. As a result, they may affect both densification and grain growth. In general, there is a decrease in open porosity after the heat treatments (Fig. 2). However, MgO doping does not seem to affect the densification of the matrix since both types of

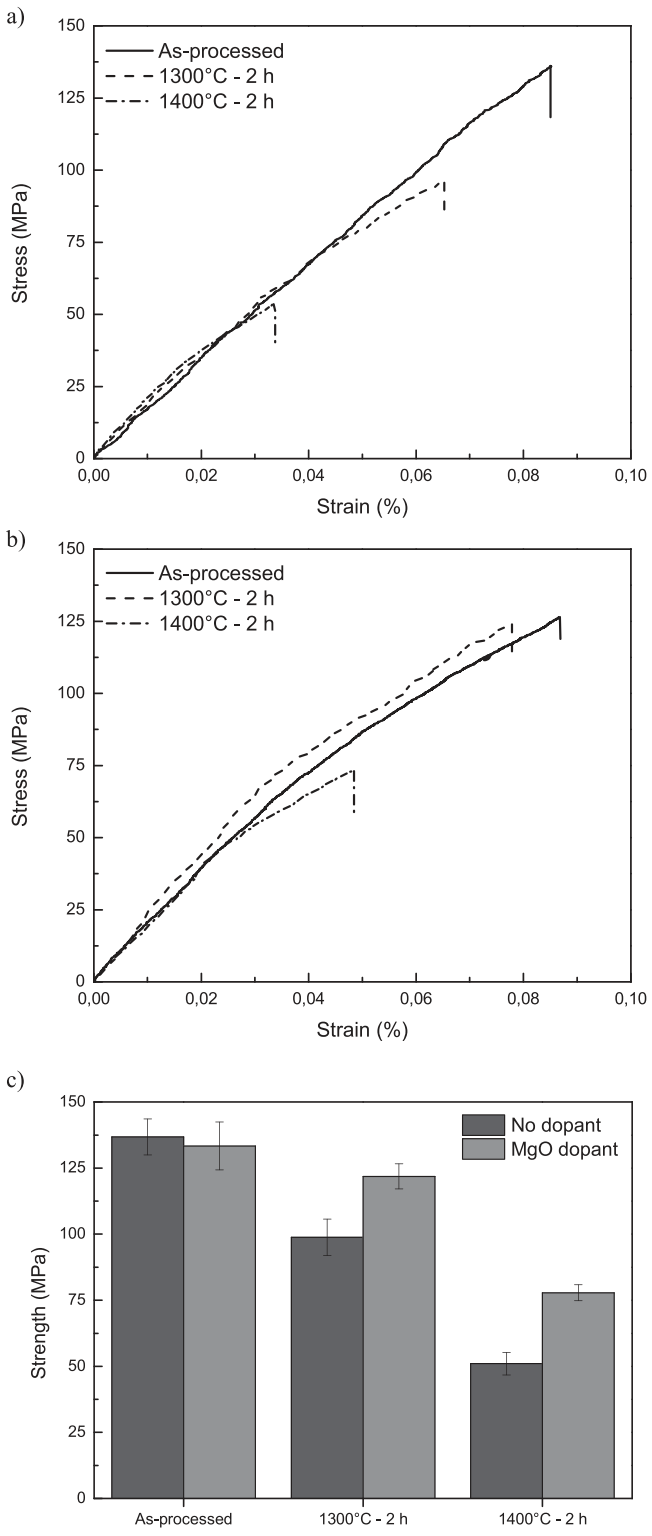

Fig. 7. Uniaxial tensile test of minicomposites before (as-processed) and after 2 h exposures to 1300 °C and 1400 °C. Example stress-strain curves for minicomposites (a) without and (b) with MgO dopant. (c) Measured tensile strength for both composite types.

composite show very similar porosity decrease after the heat treatments. In the literature, there are conflicting results regarding the effect of MgO on the densification of alumina. In this regard, MgO dopant was shown to increase [19,25,26], decrease [27] or have no influence [19,26] on the densification of alumina. Here it should also be considered that part of the MgO from the matrix diffuses into the fibers (Fig. 6). Furthermore, the fibers can also constrain the matrix densification since they are already dense.

Main differences between minicomposites with and without MgO doping can be seen when analyzing the grain growth after the heat treatments. Since MgO diffuses to the fiber center, it partially hinders the extensive fiber grain growth at temperatures above 1300 °C. As a result, MgO-doped composites show fewer abnormal grains (comparison between Figs. 3 and 4) and overall smaller grains with narrower distribution (Fig. 5) in comparison to non-doped minicomposites after the heat treatments. The effect of the MgO doping on the fibers is also probably dependent on the amount of MgO introduced to the alumina powder used for the consolidation of the matrix. Although not investigated in this work, it is presumed that lower amounts of MgO would result in lower hindering of fiber grain growth since the doping was initially in the matrix. However, attention should be taken for higher amounts of MgO. For instance, the formation of a spinel second phase has been reported when doping alumina with 500 ppm or higher amounts of MgO [16]. In this sense, the formation of a second phase could influence other properties of the composite.

The effect of the outward diffusion of Si from fibers to matrix is also evident in the grain size analysis. Because of this outward diffusion, the peripheral region of the fibers is more susceptible to grain growth. Thus, there is a clear difference between the grain size distributions of fiber center and rim of non-doped minicomposites. Similar observations were made by Schmücker et al. when comparing the grain growth of Nextel 610 fibers alone and embedded in a pure alumina matrix [12]. It should be noted that differences between fiber rim and center are also detected in MgO-doped samples even though Mg seems to be evenly distributed in the fibers after the heat treatment at 1400 °C (Fig. 6). Gavrilov et al. showed that co-doping with Mg and Si is more effective against alumina grain growth, because they increase the solubility of each other in alumina [16]. Therefore, the outward diffusion of Si also influences the grain growth in the fiber peripheral region of MgO-doped minicomposites. Then again, these composites showed smaller grains in the fiber rim when compared to non-doped composites.

Considering that both composite types show very similar as-processed microstructure, their tensile strength is also comparable in the as-processed state (Fig. 7). However, the aforementioned microstructural changes can have a direct impact on the mechanical properties of the composites after the heat treatments. Further densification of the matrix can lead to embrittlement, while fiber degradation can lead to strength decrease in Ox-CMCs [4]. Strength loss was observed for both types of composites, but MgO-doped samples showed much higher strength retention. As previously mentioned, MgO-doped and non-doped minicomposites showed very similar porosity decrease after the heat treatments. Therefore, it can be expected that they will show similar crack propagation mechanisms when loaded. Hence, the main difference between the heat treated minicomposites lies on the microstructure of the fibers. Because the inward diffusion of Mg decreases fiber grain growth, and due to the fact that the strength of polycrystalline oxide fibers is inversely proportional to their grain sizes, MgO-doped minicomposites show lower fiber degradation. Obviously, lower fiber degradation will lead to the higher strength retention of the MgO-doped composites. The effect of fiber degradation on the tensile strength of composites is more expressive in minicomposites since all fibers are in the direction of the load. Nevertheless, similar effects are to be expected for 2D- or 3D-reinforced Ox-CMCs.

5. Conclusions

In the present study, the applicability of matrix doping for the production of Ox-CMCs with improved thermal stability was investigated. For that, minicomposites containing Nextel 610 fibers and a porous alumina matrix doped with 480 ppm of MgO were produced and compared to non-doped minicomposites. The minicomposites were

evaluated regarding their microstructure and mechanical properties before and after heat treatments. In the as-produced state, the different minicomposites showed very similar microstructure and tensile strength of about 135 MPa. After the thermal exposures, reduction of the open porosity, grain growth and strength loss were observed. In addition, element diffusion between fibers and matrix take place, which affect the aforementioned property changes.

The elemental analysis of MgO-doped minicomposites showed that, during the heat treatments, Mg diffuses from the matrix to the fibers while Si diffuses from the fibers to the matrix. Due to the faster diffusion of Mg, an almost even distribution of Mg is observed, as opposed to Si, which shows constant concentration in the fiber center decreasing towards the fiber rim and matrix. Because of this inward diffusion of Mg, the co-doping of MgO and SiO_2 reduced the excessive grain coarsening of the fibers. As a result, MgO-doped minicomposites showed narrower fiber grain size distributions and average grain sizes (considering fiber center and rim) around 31% and 27% smaller than non-doped minicomposites after exposure to 1300 °C and 1400 °C, respectively. On the other hand, the further densification of the matrices did not seem to be influenced by the presence of MgO. Due to these microstructural changes, the tensile strength of all minicomposites decreased after the heat treatments. The suppression of fiber grain growth in MgO-doped minicomposites resulted in lower strength loss in comparison to non-doped composites. Therefore, the doping of alumina matrices with MgO can be a promising alternative to produce Ox-CMCs with enhanced thermal stability without reducing their room-temperature properties.

Declaration of Competing Interest

The authors declare that they have no known competing financial interests or personal relationships that could have appeared to influence the work reported in this paper.

Acknowledgments

The authors would like to thank the German Research Foundation (DFG) for the financial support under the grants TU 364/5-1 and KU 3122/3-1. Special thanks to Mr. Omar Safouri for his helpful assistance in the preparation of specimens.

References

[1] K. Tushtev, R.S.M. Almeida, Oxide/oxide CMCs – porous matrix composite systems; composites with interface coatings, in: P.W.R. Beaumont, C.H. Zweben (Eds.), Comprehensive Composite Materials II, Elsevier, Oxford, 2018, pp. 130–157.
[2] F.W. Zok, Developments in oxide fiber composites, J. Am. Ceram. Soc. 89 (11) (2006) 3309–3324.
[3] D.M. Wilson, D.C. Lueneburg, S.L. Lieder, High temperature properties of Nextel 610 and alumina-based nanocomposite fibers, in: J.B. Wachtman Jr. (Ed.), Proceedings of 17th Annual Conference on Composites and Advanced Ceramic Materials: Ceramic Engineering and Science, John Wiley & Sons, Inc., 2008, pp. 609–21.
[4] H. Liu, C. Pei, J. Yang, Z. Yang, Influence of long-term thermal aging on the microstructural and tensile properties of all-oxide ceramic matrix composites, Ceram. Int. 46 (9) (2020) 13989–13996.
[5] E. Volkmann, K. Tushtev, D. Koch, C. Wilhelmi, J. Göring, K. Rezwan, Assessment of three oxide/oxide ceramic matrix composites: mechanical performance and effects of heat treatments, Compos. Part A: Appl. Sci. Manuf. 68 (0) (2015) 19–28.
[6] R.A. Simon, R. Danzer, Oxide fiber composites with promising properties for high-temperature structural applications, Adv. Eng. Mater. 8 (11) (2006) 1129–1134.
[7] R.S.M. Almeida, E.L. Bergmüller, B.G.F. Eggert, K. Tushtev, T. Schumacher, H. Lührs, B. Clauß, G. Grathwohl, K. Rezwan, Thermal exposure effects on the strength and microstructure of a novel mullite fiber, J. Am. Ceram. Soc. 99 (5) (2016) 1709–1716.
[8] M. Schmücker, F. Flucht, P. Mechnich, Degradation of oxide fibers by thermal overload and environmental effects, Mater. Sci. Eng.: A 557 (0) (2012) 10–16.
[9] R.S. Hay, G.E. Fair, T. Tidball, Fiber strength after grain growth in Nextel 610 alumina fiber, J. Am. Ceram. Soc. 98 (6) (2015) 1907–1914.
[10] Z.R. Xu, K.K. Chawla, X. Li, Effect of high temperature exposure on the tensile strength of alumina fiber Nextel 610, Mater. Sci. Eng.: A 171 (1) (1993) 249–256.
[11] P.E. Cantonwine, Strength of thermally exposed alumina fibers – Part I. Single filament behavior, J. Mater. Sci. 38 (3) (2003) 461–470.
[12] M. Schmücker, P. Mechnich, Microstructural coarsening of NextelTM 610 fibers embedded in alumina-based matrices, J. Am. Ceram. Soc. 91 (4) (2008) 1306–1308.
[13] M. Schmücker, P. Mechnich, Improving the microstructural stability of NextelTM 610 alumina fibers embedded in a porous alumina matrix, J. Am. Ceram. Soc. 93 (7) (2010) 1888–1890.
[14] E. Volkmann, M.D. Barros, K. Tushtev, W.E.C. Pritzkow, D. Koch, J. Göring, C. Wilhelmi, G. Grathwohl, K. Rezwan, Influence of the matrix composition and the processing conditions on the grain size evolution of Nextel 610 fibers in ceramic matrix composites after heat treatment, Adv. Eng. Mater. 17 (5) (2015) 610–614.
[15] P. Milak, F.D. Minatto, C. Faller, A. da Noni, O.R.K. Montedo, The influence of dopants in the grain size of alumina – a review, Mater. Sci. Forum 820 (2015) 280–284.
[16] K.L. Gavrilov, S.J. Bennison, K.R. Mikeska, R. Levi-Setti, Role of magnesia and silica in alumina microstructure evolution, J. Mater. Sci. 38 (19) (2003) 3965–3972.
[17] I. MacLaren, R.M. Cannon, M.A. Gülgün, R. Voytovych, N. Popescu-Pogrion, C. Scheu, U. Täffner, M. Rühle, Abnormal grain growth in alumina: synergistic effects of yttria and silica, J. Am. Ceram. Soc. 86 (4) (2003) 650–659.
[18] K. Bodišová, D. Galusek, P. Švančárek, V. Pouchlý, K. Maca, Grain growth suppression in alumina via doping and two-step sintering, Ceram. Int. 41 (9, Part B) (2015) 11975–11983.
[19] S. Pal, A.K. Bandyopadhyay, S. Mukherjee, B.N. Samaddar, P.G. Pal, Function of magnesium aluminate hydrate and magnesium nitrate as MgO addition in crystal structure and grain size control of α-Al_2O_3 during sintering, Bull. Mater. Sci. 33 (1) (2010) 55–63.
[20] R.S.M. Almeida, T.F.S. Pereira, K. Tushtev, K. Rezwan, Obtaining complex-shaped oxide ceramic composites via ionotropic gelation, J. Am. Ceram. Soc. 102 (1) (2019) 53–57.
[21] H. Farhandi, M.N. Karim, R.S.M. Almeida, K. Tushtev, K. Rezwan, Increasing the tensile strength of oxide ceramic matrix mini-composites by two-step sintering, J. Am. Ceram. Soc. (2021).
[22] R.H. Doremus, Diffusion in alumina, J. Appl. Phys. 100 (10) (2006), 101301.
[23] J. Kundin, H. Farhandi, K.P. Ganesan, R.S.M. Almeida, K. Tushtev, K. Rezwan, Phase-field modeling of grain growth in presence of grain boundary diffusion and segregation in ceramic matrix mini-composites, Comput. Mater. Sci. 190 (2021), 110295.
[24] S.J. Bennison, M.P. Harmer, Effect of MgO solute on the kinetics of grain growth in $A_{12}O_3$, J. Am. Ceram. Soc. 66 (5) (1983) C-90–C-92.
[25] K.A. Berry, M.P. Harmer, Effect of MgO solute on microstructure development in Al_2O_3, J. Am. Ceram. Soc. 69 (2) (1986) 143–149.
[26] T. Ikegami, K. Eguchi, Two kinds of roles of MgO in the densification and grain growth of alumina under various atmospheres: sensitive and insensitive roles to the experimental procedures, J. Mater. Res. 14 (2) (1999) 509–517.
[27] B.N. Kim, K. Hiraga, K. Morita, H. Yoshida, Y. Kagawa, Light scattering in MgO-doped alumina fabricated by spark plasma sintering, Acta Mater. 58 (13) (2010) 4527–4535.